

Disorders of the Nervous System

# Investigating the Role of Rhodopsin *F45L* Mutation in Mouse Rod Photoreceptor Signaling and Survival

Deepak Poria,<sup>1</sup> Alexander V. Kolesnikov,<sup>1</sup> Tae Jun Lee,<sup>5</sup> David Salom,<sup>1</sup> Krzysztof Palczewski,<sup>1,2,3,4</sup> and Vladimir J. Kefalov<sup>1,3</sup>

<https://doi.org/10.1523/ENEURO.0330-22.2023>

<sup>1</sup>Department of Ophthalmology, Gavin Herbert Eye Institute, University of California, Irvine, CA 92697, <sup>2</sup>Department of Chemistry, University of California, Irvine, CA 92697, <sup>3</sup>Department of Physiology and Biophysics, University of California, Irvine, CA 92697, <sup>4</sup>Department of Molecular Biology and Biochemistry, University of California, Irvine, CA 92697, and <sup>5</sup>Department of Ophthalmology and Visual Sciences, Washington University School of Medicine, Saint Louis, MO 63110

## Abstract

Rhodopsin is the critical receptor molecule which enables vertebrate rod photoreceptor cells to detect a single photon of light and initiate a cascade of molecular events leading to visual perception. Recently, it has been suggested that the F45L mutation in the transmembrane helix of rhodopsin disrupts its dimerization *in vitro*. To determine whether this mutation of rhodopsin affects its signaling properties *in vivo*, we generated knock-in mice expressing the rhodopsin F45L mutant. We then examined the function of rods in the mutant mice versus wild-type controls, using *in vivo* electroretinography and transretinal and single cell suction recordings, combined with morphologic analysis and spectrophotometry. Although we did not evaluate the effect of the F45L mutation on the state of dimerization of the rhodopsin *in vivo*, our results revealed that F45L-mutant mice exhibit normal retinal morphology, normal rod responses as measured both *in vivo* and *ex vivo*, and normal rod dark adaptation. We conclude that the F45L mutation does not affect the signaling properties of rhodopsin in its natural setting.

**Key words:** electroretinogram; phototransduction; retinal degeneration; rhodopsin; rods

## Significance Statement

Absorption of a photon by the visual chromophore produces conformational changes in rhodopsin to open up a transducin-binding pocket and initiate the downstream signaling. The most abundantly expressed form of rhodopsin is its dimeric configuration, which is disrupted *in vitro* by the F45L mutation. Here, we show that mouse rods expressing mutant F45L rhodopsin exhibit no changes in sensitivity, response kinetics, or chromophore reconstitution compared with the rods of mice expressing wild-type rhodopsin. Our findings indicate that the F45L mutation does not affect the functional properties of the visual pigment rhodopsin. Future studies will be required to determine how the F45L mutation affects rhodopsin dimerization in the intact rod photoreceptors.

## Introduction

The visual pigment rhodopsin, a prototype G-protein-coupled receptor (GPCR; Palczewski, 2006), mediates probably the most sensitive sensory transduction, the detection of a single photon of light by the visual system

(Baylor et al., 1979; Rieke, 2000). This high sensitivity is made possible by the substantial amplification of the rod transduction cascade following photoactivation of the rhodopsin chromophore (Pugh and Lamb, 1993; Arshavsky and Burns, 2014; Yue et al., 2019). It has been established that

Received August 19, 2022; accepted January 24, 2023; First published February 21, 2023.

The authors declare no competing financial interests.

Author contributions: K.P. and V.J.K. designed research; D.P., A.V.K., T.J.L., and D.S. performed research; K.P. and V.J.K. contributed unpublished reagents/analytic tools; D.P., A.V.K., T.J.L., D.S., K.P., and V.J.K. analyzed data; D.P., A.V.K., and V.J.K. wrote the paper.

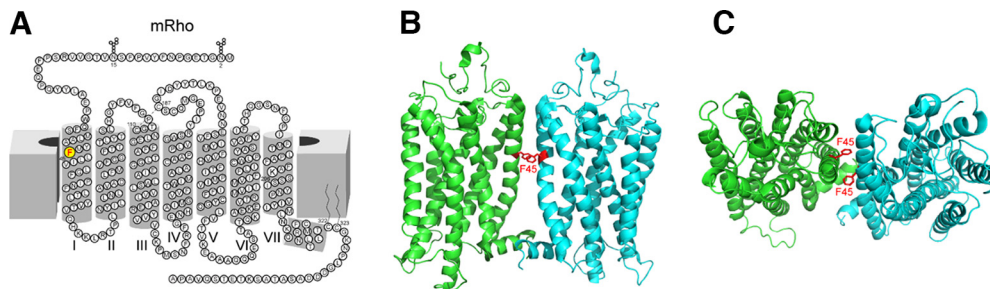


**Figure 1.** The  $Rho^{F45L}$  knock-in mutation. A 2D cartoon of mouse rhodopsin showing the mutation site at amino acid position 45 in the transmembrane helix I, where phenylalanine is replaced by leucine in the  $Rho^{F45L}$  KI mice (A). Side (B) and axial (C) views of the 3D structure of bovine rhodopsin's dimer as determined by cryo-electron microscopy (PDB ID 6OFJ), highlighting the position of F45.

even a single rhodopsin molecule (Fig. 1A) expressed *in vitro* can initiate downstream intracellular signaling (Ernst et al., 2007; Whorton et al., 2007, 2008; Tsukamoto et al., 2010). These findings indicate that rhodopsin can function as a monomeric unit. However, *in vitro* purification studies have shown that rhodopsin forms oligomers, among which dimers are the most prevalent (Fig. 1B; Sung et al., 1991b; Fotiadis et al., 2006; Jastrzebska et al., 2006; Park et al., 2008). Moreover, when expressed abundantly, the recombinant rhodopsin exists as a dimer in cultured cells as well (Sung et al., 1991b; Kota et al., 2006). A recent study of the morphologic structure of the disk surface of the rod outer segment showed that rhodopsin molecules organize as rows of dimers on the disk membrane (Zhao et al., 2019). However, several mutations of the rhodopsin molecule,  $F45L$ ,  $V209M$ , and  $F220C$ , have been shown to disrupt the dimerization of the protein *in vitro* (Sung et al., 1991b; Kaushal and Khorana, 1994; Ploier et al., 2016). One of these studies (Kaushal and Khorana, 1994) reported the binding affinity of monomeric rhodopsin for transducin to be compromised. These rhodopsin mutations have been detected in patients with retinal degenerative disease and previously were interpreted to be associated with the disease phenotype (Sung et al., 1991a; Berson et al., 2002). However, recent evidence ruled out a role for either the  $F45L$  or  $F220C$  mutations in retinal degeneration (Vincent et al., 2013; Lewis et al., 2020).

Studies with mutant  $F45L$  rhodopsin have shown that this rod visual pigment can translocate and incorporate successfully into the cell membrane and rod outer

segments (Ploier et al., 2016). Specific sites in the transmembrane domains of the rhodopsin partner molecules have been speculated to interact within the dimers through various states of activation of the receptor (Fig. 1C; Salom et al., 2006; Scheerer et al., 2008; Cordomi and Perez, 2009; Choe et al., 2011). Additionally, the individual rhodopsin subunits distinctly rearrange within a dimer complex as compared with the single molecular state (Cordomi and Perez, 2009). These structural modifications present possibilities for alterations in target binding sites, potentially triggering allosteric mechanisms that could be involved in modulation of the rhodopsin activity.

Rhodopsin is the prototypical member of GPCR subfamily A, among which negative allosteric interactions between homomeric partners have been shown previously (Springael et al., 2005; Urizar et al., 2005; Rivero-Muller et al., 2010). However, potential allosteric interactions within rhodopsin dimers and their effect on visual perception remain uncharacterized.

In this study, we sought to investigate the role of the F45 rhodopsin residue in rhodopsin signaling by studying the light response sensitivity, kinetics, and survival of rods in mice carrying the  $Rho^{F45L}$  knock-in mutation. In the process of preparing this manuscript, another group published a study on an unrelated F45L mutant mouse line that reported some findings similar to ours (Lewis et al., 2020).

## Materials and Methods

### Animals

The  $Rho^{F45L}$  KI mutant mice were generated commercially (Ingenious Targeting Laboratory) on a C57Bl/6 background. The codon substitution TTC>CTC at position 45 was confirmed by sequencing. The animals were maintained in a 12 h/12 h light/dark cycle at all times. Both male and female animals of three months of age were used in the experiments, unless age is specified otherwise.

### Electrophysiology

For physiology experiments, all animals were dark-adapted overnight before the day of the experiment. For *in vivo* ERG recordings, the animals were anaesthetized using a cocktail

This research was supported in part by National Institutes of Health (NIH) Grants R01EY030912 (to V.J.K.) and R01EY030873 (to K.P.). The authors also acknowledge support from an Research to Prevent Blindness unrestricted grant to the Department of Ophthalmology, University of California, Irvine.

**Acknowledgments:** We thank members of the Kefalov and Palczewski laboratories for their helpful comments on this manuscript. K.P. is the Irving H. Leopold Chair of Ophthalmology at the Gavin Herbert Eye Institute, Department of Ophthalmology, University of California, Irvine.

Correspondence should be addressed to Vladimir J. Kefalov at [vkefalov@uci.edu](mailto:vkefalov@uci.edu).

<https://doi.org/10.1523/ENEURO.0330-22.2023>

Copyright © 2023 Poria et al.

This is an open-access article distributed under the terms of the Creative Commons Attribution 4.0 International license, which permits unrestricted use, distribution and reproduction in any medium provided that the original work is properly attributed.

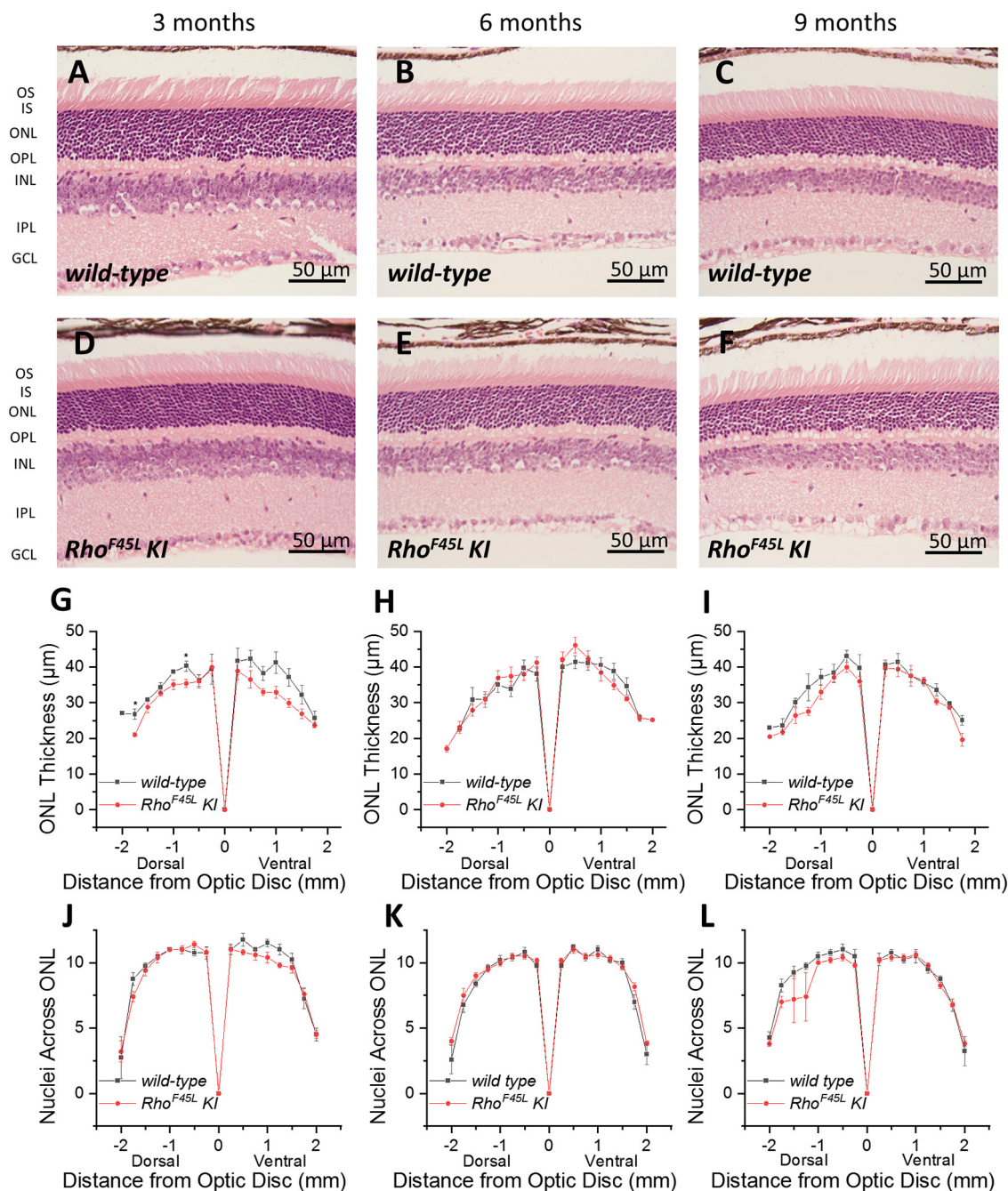


**Figure 2.** Effect of the *Rho<sup>F45L</sup>* knock-in mutation on photoreceptor morphology. Representative images from retinas of three-, six-, and nine-month-old *wild-type* mice (**A–C**, respectively), and age-matched *Rho<sup>F45L</sup> KI* mice (**D–F**, respectively). Quantitative spider plots of ONL thickness as a function of distance from the optic nerve disk from *wild-type* mice (black;  $n = 4$  each), and from *Rho<sup>F45L</sup> KI* mice (red;  $n = 5, 4, 5$ ) measured at three-, six-, and nine-month time points (**G–I**, respectively). Quantitative spider plots of the number of photoreceptor nuclei per column in the ONL as a function of distance from the optic nerve disk from *wild-type* mice (black;  $n = 4$  each), and from *Rho<sup>F45L</sup> KI* mice (red;  $n = 5, 4, 5$ ) measured at three-, six-, and nine-month time points (**J–L**, respectively). Error bars indicate SEM; \* $p < 0.05$ .

of ketamine (100 mg/kg) and xylazine (4 mg/kg). Pupils were dilated with a drop of 1% atropine sulfate. The mouse body temperature was maintained at 37°C with a heating pad connected to a controller. Full-field ERG responses to calibrated green (530 nm) LED light were recorded from both eyes by contact corneal electrodes held in place by a drop of Gonak

solution (Akorn). ERGs were recorded using a clinical ERG setup (LKC Technologies; Model UBA-4200c) adapted for mice.

Rod ERG a-wave fractional flash sensitivity ( $S_f$ ) was calculated from the linear part of the intensity-response curve, as follows:

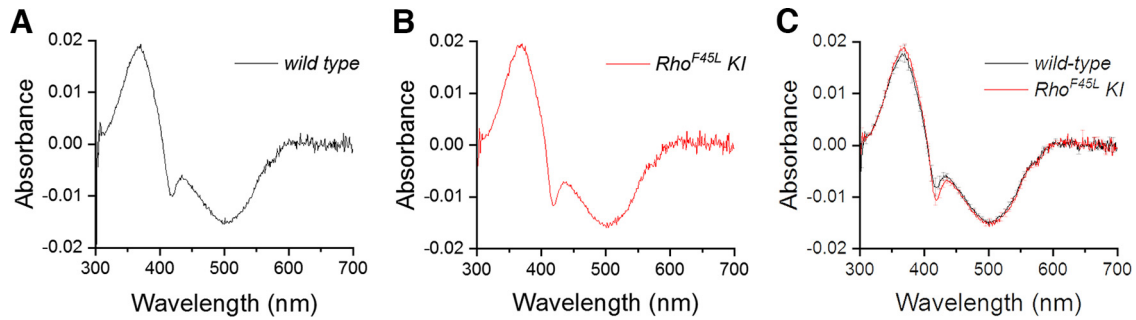


**Figure 3.** Effect of the *Rho*<sup>F45L</sup> knock-in mutation on rhodopsin expression. Representative difference absorbance spectra of rhodopsin (before vs after bleaching) from *wild-type* mice (A) and *Rho*<sup>F45L</sup> KI mice (B). Averaged spectra from *wild-type* mice (black; *n* = 2 eyes) and *Rho*<sup>F45L</sup> KI mice (red; *n* = 2 eyes; C). All measurements were done from three-month-old animals.

$$S_f = \frac{R}{R_{max} \cdot I},$$

where *R* is the amplitude of the rod a-wave dim flash response, *R*<sub>max</sub> is the maximum amplitude of the rod a-wave response for that eye (determined at 23.5 cd·s m<sup>-2</sup>), and *I* is the flash strength. The sensitivity of rods was first determined in the dark. To monitor the postbleach recovery of *R*<sub>max</sub> and *S*<sub>f</sub>, more than 90% of rhodopsin was bleached with a 35-s exposure to 520-nm LED light focused at the surface of the cornea. The bleached pigment fraction was calculated with the following equation:

$$F = 1 - e^{(-I \cdot P \cdot t)},$$

where *F* is the fraction of rhodopsin bleached, *t* is the duration of the light exposure (s), *I* is the bleaching light intensity of 520-nm LED light (1.3 × 10<sup>8</sup> photons μm<sup>-2</sup> s<sup>-1</sup>), and *P* is the photosensitivity of mouse rods at the wavelength of peak absorbance (5.7 × 10<sup>-9</sup> μm<sup>2</sup>; Woodruff et al., 2004). Mice were re-anesthetized once after 30 min with a lower dose of ketamine (~1/3 of the initial dose) and a small drop of PBS solution was gently applied to their eyes with a plastic syringe to protect them from drying and to maintain contact with the recording electrodes.

For *ex vivo* transretinal recordings, the animals were euthanized with CO<sub>2</sub> and then their eyes were enucleated under dim red light followed by dissection under infrared illumination. The dissection was performed in a Petri dish containing oxygenated Ames' medium (Sigma). First, the eyeballs were cut close to the limbus, then the retina was gently detached from the posterior eye cup by tearing the sclera and retinal pigmented epithelium (RPE), using forceps. The retinas were stored in oxygenated Ames' medium in a dark chamber at room temperature until recording. Recordings were conducted using previously described methods (Vinberg and Kefalov, 2015). The recordings were made using a closed chamber where the retina was mounted with photoreceptors facing up. The recording chamber was continuously supplied with oxygenated Ames' medium at a flow rate of 3–5 ml/min. For isolating the photoreceptor component of the transretinal response, 50 μM DL-AP<sub>4</sub> (Tocris) and 100 μM BaCl<sub>2</sub> (Sigma) were included in the Ames' medium. The chamber temperature was maintained at 35–36°C, and retinas were allowed to adapt to the chamber temperature for at least 15 min before the start of the recordings. *Ex*

*in vivo* ERG recordings were made by presenting light flashes produced by computer-controlled LEDs (Thor Labs). The signals were amplified using a differential amplifier (Warner Instruments), low-pass filtered at 300 Hz (Krohn Hite Corp.), digitized using Digidata 1440 (Molecular Devices), and recorded on a computer at a sampling frequency of 10 kHz, using pClamp 10 software.

For single-cell suction recordings from rod outer segments, following dissection of the eyes under infrared illumination, the retinas were chopped into small pieces in a dish containing oxygenated Locke's solution (in mM: 112.5 NaCl, 3.6 KCl, 2.4 MgCl<sub>2</sub>, 1.2 CaCl<sub>2</sub>, 10 HEPES, 20 NaHCO<sub>3</sub>, 0.02 EDTA, 3.0 Na<sub>2</sub>-succinate, 0.5 Na-glutamate, 10.0 glucose, and 0.1% MEM vitamins). The retinal pieces were then transferred to an open chamber maintained at 35–36°C with a continuous supply of heated Locke's solution at 2–3 ml/min. Borosilicate glass pipettes, pulled to ~1-μm inner diameter over a heated filament (Sutter Instruments), fire-polished, and filled with electrode solution (in mM: 140 NaCl, 3.6 KCl, 2.4 MgCl<sub>2</sub>, 1.2 CaCl<sub>2</sub>, 3.0 HEPES, 0.02 EDTA, and 10.0 glucose; pH adjusted to 7.4 with NaOH), were used in these experiments. Single rod outer segments were approached under infrared visual control and gently drawn into the glass pipette. Recordings were made by presenting flash stimuli produced by computer-controlled LEDs (Thor Labs). Signals were amplified using Axopatch 200B, low-pass filtered at 10 Hz (Krohn Hite Corp.), digitized using Digidata 1440 (Molecular Devices), and recorded on a computer at a sampling frequency of 10 kHz, using pClamp 10 software.

### Data analysis

Data were analyzed using Clampfit 10.7 (Molecular Devices), Microsoft Excel and Origin 9.8.5 (64 bit, SR2, OriginLab) and presented as mean ± SEM *p*-values of <0.05 (Student's *t* test) were considered significant. The intensity-response relationships data were fitted by a hyperbolic Naka–Rushton function using the following equation:

$$\frac{R}{R_{max}} = \frac{I^n}{I^n + I_{1/2}^n},$$

where *R* is the flash response, *R*<sub>max</sub> is the maximum response amplitude, *I* is the flash intensity, *n* is the Hill

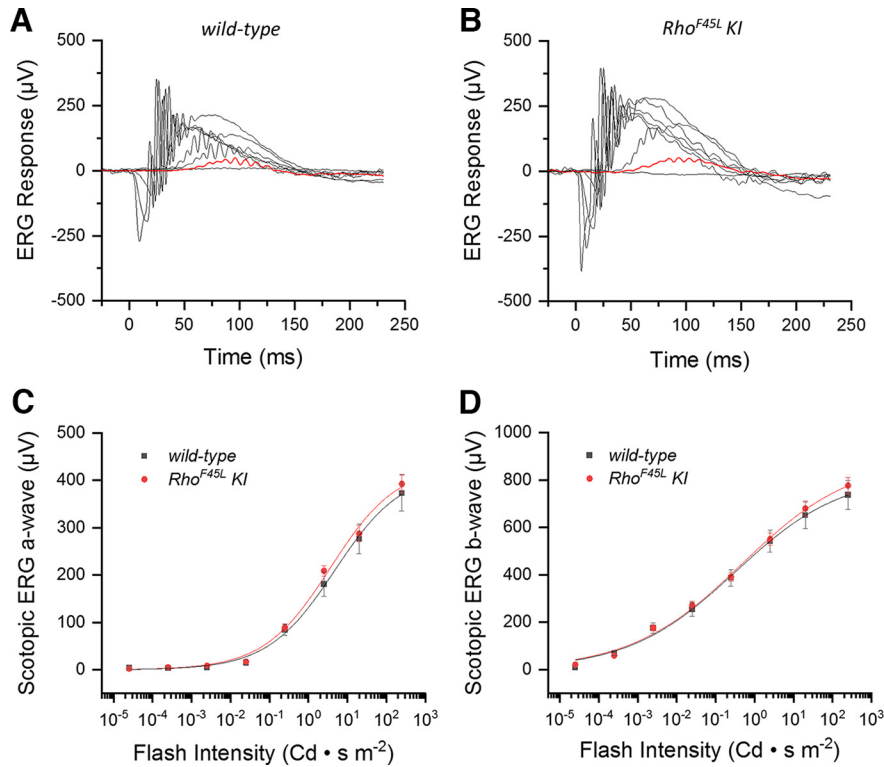


**Figure 4.** Effect of the *Rho<sup>F45L</sup>* knock-in mutation on *in vivo* scotopic ERG responses. Representative families of ERG responses to flashes of increasing intensity ( $\text{Cd} \cdot \text{s m}^{-2}$ :  $2.5 \times 10^{-5}$ ,  $2.5 \times 10^{-4}$ ,  $2.5 \times 10^{-3}$ ,  $2.5 \times 10^{-2}$ , 0.25, 2.5, 20, and 250) recorded in scotopic conditions from *wild-type* mice (**A**) and *Rho<sup>F45L</sup> KI* mice (**B**). For comparison, the responses to a flash of  $2.5 \times 10^{-4} \text{ Cd} \cdot \text{s m}^{-2}$  are highlighted in red in the two panels. Population-averaged a-wave response amplitudes (**C**) and b-wave response amplitudes (**D**) from groups of *wild-type* mice (black;  $n=5$ ) and *Rho<sup>F45L</sup> KI* mice (red;  $n=5$ ) are plotted together as a function of flash intensity. Error bars indicate SEM. Differences in **C** and **D** were not significant ( $p > 0.05$ ) for all data points. All measurements were done from three-month-old mice.

coefficient, and  $I_{1/2}$  is the intensity to produce half-saturating response. The light adaptation data were fitted by a modified Weber–Fechner function, as follows:

$$\frac{S_f}{S_{fDA}} = \frac{I_0^n}{I_0^n + I^n}$$

where  $S_f$  is the rod sensitivity (as defined above),  $S_{fDA}$  is the rod sensitivity in darkness,  $n$  is a slope factor (Hill coefficient),  $I$  is the background light intensity (in photons  $\mu\text{m}^{-2} \text{ s}^{-1}$ ), and  $I_0$  is the background light intensity needed to reduce the sensitivity to 50% of that in darkness.

### Morphology and microscopy

For morphologic studies, the eyeballs from three-, six-, and nine-month-old animals were fixed overnight in 4% paraformaldehyde at 4°C, embedded in paraffin, and then sectioned into 10- $\mu\text{m}$ -thick sections. For identification of the dorsal and ventral sides of the retinas, the eyes were

marked on the ventral surface of the cornea by a high-temperature cautery pen. Retinal sections were stained with hematoxylin and eosin (H&E) to label the nuclei. The stained sections were imaged at 40 $\times$  magnification using an Olympus BX51 microscope. The outer and inner nuclear layer thickness was measured using ImageJ software (NIH).

### Rhodopsin measurements

Mouse eyes were enucleated in darkness under dim red light. Each eye was flash-frozen on dry ice immediately after enucleation. Rhodopsin was extracted with 20 mM HEPES, pH 7.4, containing 10 mM n-dodecyl- $\beta$ -maltoside and 5 mM freshly neutralized  $\text{NH}_2\text{OH}\cdot\text{HCl}$ , as described previously (Palczewska et al., 2018). Briefly, the tissue was homogenized with 0.9 ml of buffer in a 2-ml Dounce tissue homogenizer (Kontes Glass Co) and shaken for 5 min at 4°C. The sample was then centrifuged at  $17,200 \times g$  for 5 min at 4°C. The supernatant was collected, the pellet was extracted a second time with 0.9 ml of buffer, and the combined supernatants were filtered through a 0.22- $\mu\text{m}$  polyethersulfone membrane. Absorbance spectra were recorded using a Varian Cary 50-Scan UV-Vis spectrophotometer (Varian Australian Pty Ltd.); the sample was used as blank, then it was bleached for 5 min with a white-light, 875-

**Table 1: Scotopic visual behavior test results**

	Visual acuity (cyc/°)	Contrast threshold (%)	N
<i>wild type</i>	$0.72 \pm 0.04$	$11.9 \pm 1.5$	3 mice
<i>Rho<sup>F45L</sup> KI</i>	$0.67 \pm 0.02$	$12.7 \pm 1.2$	6 mice
<i>p</i> value	$>0.05$	$>0.05$	

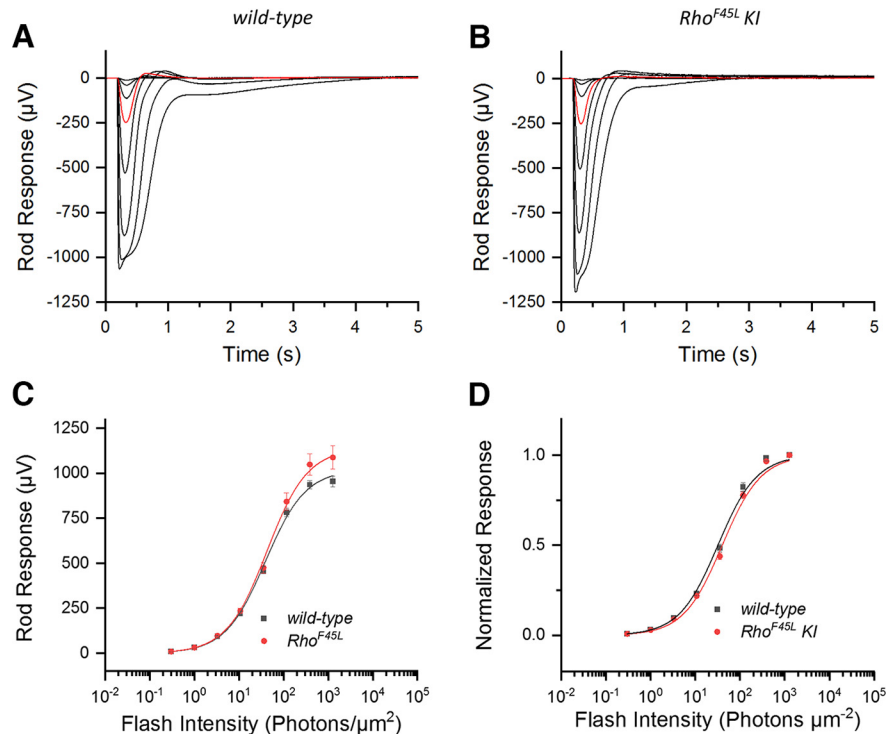


**Figure 5.** Effect of the *Rho<sup>F45L</sup>* knock-in mutation on *ex vivo* ERG rod responses. Representative families of responses to flashes of increasing intensity (photons  $\mu\text{m}^{-2}$ : 0.3, 1, 3, 10.7, 35, 117, 386, and 1271) for retinas from *wild-type* mice (**A**) and *Rho<sup>F45L</sup> KI* mutant mice (**B**). For comparison, the responses to a flash of 35 photons  $\mu\text{m}^{-2}$  are highlighted in red in both panels. Average flash response amplitudes (**C**) and average normalized flash response amplitudes (**D**) for rods from *wild-type* mice (black;  $n=5$  mice, 8 retinas) and *Rho<sup>F45L</sup> KI* mutant mice (red;  $n=6$  mice, 10 retinas) are plotted together as a function of flash intensity. Error bars indicate SEM. The lines represent curves fitted to the data using a hyperbolic Naka–Rushton function. All measurements were done from three-month-old mice.

Lumens bulb, and finally the difference absorbance spectrum was recorded immediately following a bleach. The concentration of rhodopsin was determined by the decrease in absorbance at 500 nm using the molar extinction coefficient  $\epsilon_{500\text{nm}} = 42,000 \text{ M}^{-1} \cdot \text{cm}^{-1}$ .

## Results

### *Rho<sup>F45L</sup> KI* mutation does not cause rod degeneration

*Rho<sup>F45L</sup>* expressed *in vitro* has been demonstrated to retain the capability to activate transducin; however, its binding affinity to transducin was shown to be reduced (Kaushal and Khorana, 1994). Because the loss of rhodopsin leads to photoreceptor degeneration in mice (Lem et al., 1999), we speculated that a partial loss of pigment function in the *Rho<sup>F45L</sup> KI* mouse line could also lead to rod death. First, we examined the retinal morphology at three different time points. We found that there were no detectable changes in the outer nuclear layer (ONL)

thickness in three-, six-, and nine-month-old *wild-type* mice (Fig. 2A–C, respectively) or in the age-matched *Rho<sup>F45L</sup> KI* mutant mice (Fig. 2D–F, respectively). We then quantified the ONL morphology by measuring the thickness (Fig. 2G–I) as well as by counting the nuclei per ONL column (Fig. 2J–L) at several different locations across the retina, which showed no significant differences between the two types of mice at any of the time points studied, with the exception of two different locations in the dorsal retina of three-month-old mice where we observed small but significant diminutions of 22% and 12% for the *Rho<sup>F45L</sup> KI* mice (Fig. 2G). Thus, overall, the *Rho<sup>F45L</sup> KI* mutation did not cause notable rod degeneration in the mouse retina.

### *Rho<sup>F45L</sup> KI* mutation does not affect the expression of rhodopsin in rods

The normal development and health of rods is strongly dependent on the proper level of expression of rhodopsin (Fulton

**Table 2: Transretinal recordings analysis parameters**

	$R_{\text{max}}$ (μV)	$S_f^{\text{DA}}$ ( $\times 10^{-3} \text{ phot}^{-1} \mu\text{m}^2$ )	$I_{1/2}$ (phot $\mu\text{m}^{-2}$ )	$N$
<i>wild type</i>	$954 \pm 30$	$22 \pm 1$	$39 \pm 4$	5 mice, 8 retinas
<i>Rho<sup>F45L</sup> KI</i>	$1088 \pm 64$	$21 \pm 1$	$46 \pm 4$	6 mice, 10 retinas
<i>p</i> value	0.08	0.40	0.16	

$R_{\text{max}}$ , saturated response amplitude measured at the plateau.  
 $S_f^{\text{DA}}$ , dark-adapted sensitivity.  
 $I_{1/2}$ , intensity required to produce half of the saturated response.

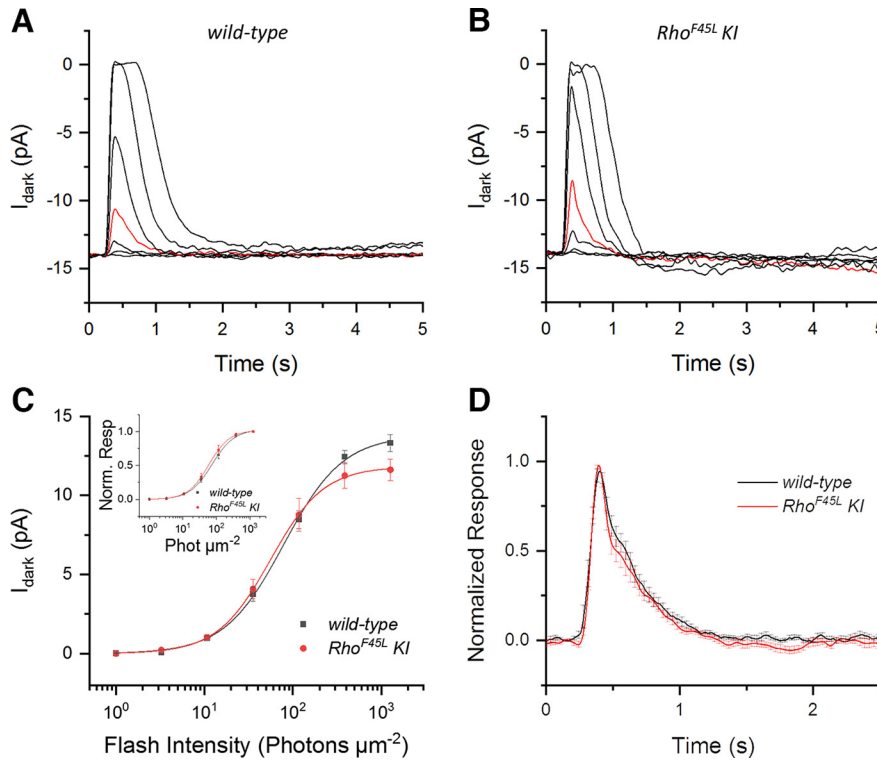


**Figure 6.** Effect of the *Rho<sup>F45L</sup>* knock-in mutation on individual rod responses. Representative families of responses of individual rods to flashes of increasing intensity (photons  $\mu\text{m}^{-2}$ : 1, 3, 10.7, 35, 117, 386, and 1271); **(A)** rods from *wild-type* mice, and **(B)** rods from *Rho<sup>F45L</sup>* knock-in mutant mice. For comparison, the responses to a flash of 35 photons  $\mu\text{m}^{-2}$  are highlighted in red in the two panels. Population-averaged flash response amplitudes **(C)** and averaged normalized flash response amplitudes **(C, inset)** for rods from *wild-type* mice (black;  $n = 14$  cells), and rods from *Rho<sup>F45L</sup>* knock-in mutant mice (red;  $n = 13$  cells) plotted together as a function of flash intensity. Error bars indicate SEM. The lines represent curves fitted to the data points using a Naka–Rushton function. **D**, Normalized averaged dim flash responses for rods from *wild-type* mice (black;  $n = 10$  cells), and from *Rho<sup>F45L</sup>* knock-in mutant mice (red;  $n = 13$  cells) plotted together for comparison of response kinetics. All measurements were done from three-month-old mice.

et al., 2009; Wen et al., 2009). Our finding that the *Rho<sup>F45L</sup>* KI mutant retina does not present detectable degeneration even at nine months of age suggests that the mutant rhodopsin is expressed at a normal (fully functional) level compared with that in *wild-type* rods. To evaluate rhodopsin expression directly, we measured absorbance spectra for eye extracts of rhodopsin from retinas of *wild-type* and *Rho<sup>F45L</sup>* KI mutant mice. We found that the *F45L* variant exhibited peak absorbance at 500 nm, similar to *wild-type* rhodopsin (Fig. 3). There were no significant differences in the quantified rhodopsin absorbance spectra for retina samples from *Rho<sup>F45L</sup>* KI mutant and *wild-type* mice, indicating that their rhodopsin levels and spectral characteristics were indistinguishable.

***Rho<sup>F45L</sup>* KI mutation does not affect the rod response**

We next tested whether the *Rho<sup>F45L</sup>* KI mutation affected the physiological response of the rods by recording *in vivo* ERG responses under scotopic conditions. We found that the rod-driven responses of *Rho<sup>F45L</sup>* KI mutant mice (Fig. 4B) were comparable to those of *wild-type* mice (Fig. 4A). Comparison of the a-wave (Fig. 4C) and b-wave (Fig. 4D) intensity-response relationships further revealed that they were essentially identical for *wild-type* and the *Rho<sup>F45L</sup>* KI mutant mice. This finding was also consistent with the results of scotopic optomotor reflex experiments performed with these mice, which showed statistically indistinguishable visual

**Table 3: Rod outer segment suction recordings analysis parameters**

	$I_{\text{dark}}$ (pA)	$S_f^{\text{DA}}$ ( $\times 10^{-3}$ phot $^{-1}$ $\mu\text{m}^2$ )	$I_{1/2}$ (phot $\mu\text{m}^{-2}$ )	$T_p$ (ms)	$T_{\text{int}}$ (ms)	$\tau_{\text{rec}}$ (ms)	$N$
<i>wild type</i>	$13 \pm 1$	$8 \pm 1$	$89 \pm 14$	$215 \pm 12$	$941 \pm 60$	$273 \pm 24$	14 cells
<i>Rho<sup>F45L</sup></i> KI	$12 \pm 1$	$10 \pm 1$	$76 \pm 15$	$227 \pm 10$	$965 \pm 39$	$357 \pm 61$	13 cells
<i>p</i> value	0.06	0.52	0.55	0.43	0.74	0.22	

$I_{\text{dark}}$ , saturated response amplitude measured at the plateau.  
 $S_f^{\text{DA}}$ , dark-adapted sensitivity.  
 $I_{1/2}$ , intensity required to produce half of the saturated response.  
 $T_p$ , time to peak of a dim flash response.  
 $T_{\text{int}}$ , integration time of the response.  
 $\tau_{\text{rec}}$ , recovery time constant during response shut off.

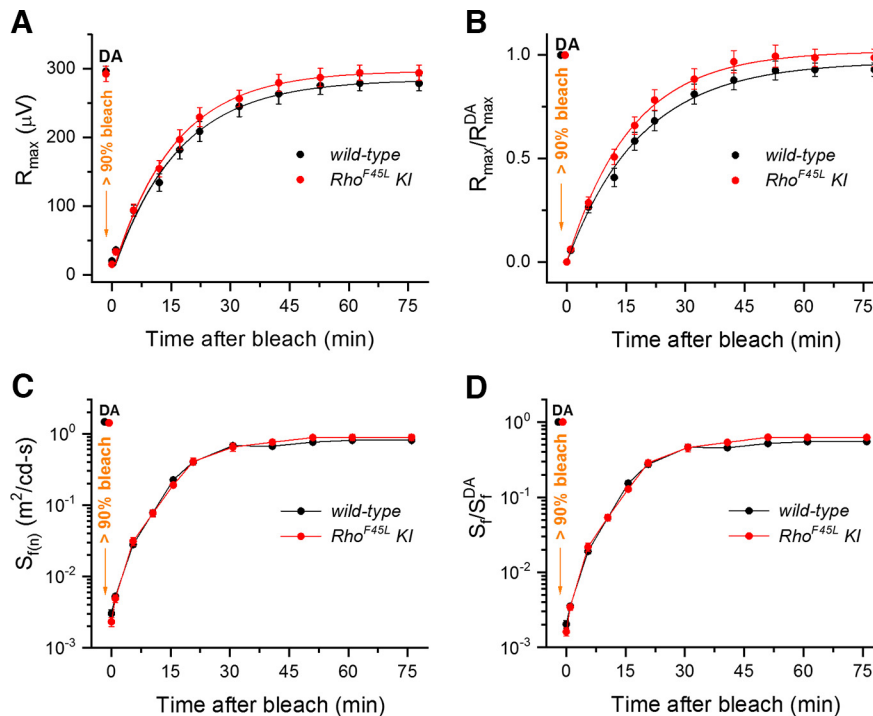


**Figure 7.** Effect of the *Rho*<sup>F45L</sup> knock-in mutation on dark adaptation of rods. Recovery of absolute (A) and normalized (B) scotopic ERG maximal a-wave amplitudes ( $R_{max}$ ; mean  $\pm$  SEM) after bleaching >90% of rhodopsin in eyes of *wild-type* mice (black,  $n = 12$ ) and *Rho*<sup>F45L</sup> knock-in mutant mice (red,  $n = 12$ ). Bleaching was achieved by a 35-s illumination with bright 520 nm LED light at time 0.  $R_{max}^{DA}$  refers to the prebleach maximal response in the dark (DA). Averaged data points were fitted with single exponential functions yielding time constants of  $18.7 \pm 0.9$  and  $16.2 \pm 0.6$  min for *wild-type* and *Rho*<sup>F45L</sup> knock-in mice, respectively. Recovery of absolute (C) and normalized (D) scotopic ERG a-wave flash sensitivity ( $S_f$ ; mean  $\pm$  SEM) after bleaching >90% of rhodopsin in the same *wild-type* mice (black,  $n = 12$ ) or *Rho*<sup>F45L</sup> knock-in mice (red,  $n = 12$ ).  $S_f^{DA}$  designates the sensitivity of dark-adapted (DA) rods. All measurements were done from three-month-old mice.

acuity and contrast sensitivity for the two groups of mice (Table 1).

We next turned to *ex vivo* ERG recordings that allow pharmacological manipulation of the retinal response to isolate its photoreceptor component. The rod responses recorded *ex vivo* were also similar for the *wild-type* and *Rho*<sup>F45L</sup> KI mutant mice (Fig. 5A,B, respectively), and had comparable maximal amplitudes and sensitivities (Table 2). The intensity-response functions for these two groups were only marginally different (Fig. 5C) and the composite sets of data were evaluated as *not* statistically different (Table 2). The normalized intensity-response relationships were also indistinguishable for the *wild-type* and *Rho*<sup>F45L</sup> KI mutant mice (Fig. 5D), demonstrating their similar photosensitivities (Table 2).

To study the kinetics of rod responses, we compared dim flash responses from single rod outer segments of *wild-type* and *Rho*<sup>F45L</sup> KI mutant mice. As expected, the response amplitudes and sensitivities were comparable between the two groups (Fig. 6A–C; Table 3). We also found that the rod dim-flash response kinetics were indistinguishable between *wild-type* and *Rho*<sup>F45L</sup> KI mutant mice (Fig. 6D), with similar times to peak, integration times, and recovery time constants for the two groups (Table 3). Thus, the overall data indicate that the *Rho*<sup>F45L</sup> KI mutation did not affect the rod light response.

### *Rho*<sup>F45L</sup> KI mutation does not affect dark adaptation of rods

Finally, to investigate a possible impact of the *Rho*<sup>F45L</sup> mutation on the ability of rods to process their rhodopsin photointermediates and regenerate their visual pigment after its substantial bleaching, we measured the kinetics of rod dark adaptation *in vivo* (Fig. 7A–D). Under these conditions, the rate of rod dark adaptation is determined by the speed of recycling of the spent visual chromophore (all-*trans*-retinal) back to its initial 11-*cis*-retinal form in the canonical RPE-dependent retinoid (visual) cycle. In accordance with the unchanged intensity-response relationship (Fig. 4C), the maximal dark-adapted (DA) scotopic ERG a-wave amplitude,  $R_{max}$ , was not affected by the *Rho*<sup>F45L</sup> substitution in this separate group of two-month-old mice ( $297 \pm 8 \mu V$  for controls vs  $293 \pm 11 \mu V$  for mutants,  $n = 12$  in each case,  $p > 0.05$ ; Fig. 7A). Rod ERG a-wave photosensitivity,  $S_f$ , was also identical in the two groups ( $1.47 \pm 0.04 \text{ m}^2 \text{ cd}\cdot\text{s}^{-1}$  for controls vs  $1.40 \pm 0.04 \text{ m}^2 \text{ cd}\cdot\text{s}^{-1}$  for mutants,  $n = 12$  in each case,  $p > 0.05$ ; Fig. 7C). The single-exponential recovery of rod-driven ERG a-wave response following exposure of the eyes to brief bright light (estimated to bleach > 90% of rhodopsin) was also unaltered, with its final postbleach levels reaching 81% and 89% for *wild-type* and mutant mice, respectively (Fig. 7B); and the lack of difference was confirmed for the comparison of the recovery of normalized scotopic



ERG a-wave sensitivity for *wild-type* and *Rho*<sup>F45L</sup> animals (Fig. 7D). We conclude that the *Rho*<sup>F45L</sup> mutation does not affect the kinetics of regeneration of rhodopsin and the dark adaptation of rods, consistent with the normal pigment levels and photoresponses in *Rho*<sup>F45L</sup> mice in the dark.

## Discussion

In this study, we investigated the possible effect of a Phe to Leu substitution mutation *F45L* in rhodopsin on the morphology and visual function of rod photoreceptors in the mouse retina. Our results demonstrate that the *Rho*<sup>F45L</sup> mutation does not lead to any changes in the function of rhodopsin; thus, the physiology, health, and survival of the rods remain unchanged. These results are consistent with recent studies by Lewis et al., 2020; where they showed that mice expressing rhodopsin *F45L*-mutants or *F220C*-mutants exhibited no change in rod physiology, protein distribution, morphology, or survival.

Our finding that the quantified absorbance of the *F45L*-mutant rhodopsin is unchanged from the wild-type rhodopsin indicates that the absolute level of rhodopsin remains unaltered in the *Rho*<sup>F45L</sup> *KI* rods. Additionally, we found that the light response amplitude and sensitivity of rods from *Rho*<sup>F45L</sup> *KI* mutant mice were essentially the same as those from wild-type mice, suggesting that the activation phase of the response is unchanged in the *Rho*<sup>F45L</sup> mutants. The amplification of the rod phototransduction cascade is directly proportional to the level of G-protein transducin  $\alpha$ -subunit in the outer segments of mammalian rods (Arshavsky et al., 2002; Sokolov et al., 2002) and depends on the overall binding affinity of transducin heterotrimer to rhodopsin (Kolesnikov et al., 2011). Thus, together these findings suggest that, not only do these mutant rods express normal levels of rhodopsin and transducin leading to efficient amplification of the transduction cascade, but also that the rhodopsin-transducin interaction and binding affinity remain normal.

We also found that the time course of dark adaptation of the rods from the mutant *Rho*<sup>F45L</sup> *KI* mice after near complete bleaching of their visual pigment was indistinguishable from that of the rods from wild-type mice. This novel observation indicates that the overall kinetics of pigment regeneration *in vivo* are not affected by the *F45L* mutation of rhodopsin. Dark adaptation of rod photoreceptors is a complex process that involves the release and reduction of the spent all-*trans*-retinal from photoactivated rhodopsin, followed by its recycling to 11-*cis*-retinal in the retinal pigmented epithelium (RPE), its return to photoreceptors, and finally binding to free opsin and formation of a Schiff base to reconstitute the ground-state rhodopsin molecule (Lamb and Pugh, 2004). The overall speed of this process is limited by the supply of fresh chromophore from the RPE to the rods (Lamb and Pugh, 2004; Wang et al., 2014). However, modulation of the thermal decay of photoactivated rhodopsin intermediates by G-protein-coupled receptor kinase 1 and arrestin 1 (Frederiksen et al., 2016) and its phosphorylation status (Kolesnikov et al., 2017) can also affect the overall time course of dark adaptation of rods. Thus, our observation that rod dark adaptation in *Rho*<sup>F45L</sup> *KI* mice is unchanged

indicates that the chromophore release, its re-isomerization in the RPE, and subsequent binding of freshly formed 11-*cis*-retinal to mutant opsin all remain normal in these animals.

Overall, our findings rule out the possibility that the *Rho*<sup>F45L</sup> mutation exerts a functionally significant allosteric modulation of rhodopsin either during signaling or during pigment regeneration in mouse rods. Additionally, we show that the mutant rods remain healthy for up to several months of age, suggesting that the *Rho*<sup>F45L</sup> mutation does not give rise to any pathologic conditions leading to photoreceptor death. These findings are consistent with recent studies and, in conjunction, support the emerging view that the *F45L* point mutation is not implicated in such hereditary diseases as retinitis pigmentosa (Vincent et al., 2013; Lewis et al., 2020). The *F45L* mutation detected in a few retinitis pigmentosa patients diagnosed earlier could possibly be a consequence of this mutation occurring coincidentally with other unidentified mutations leading to the disease, as several newer mutations implicated in inherited retinal degenerations have been identified in the following decades (Sung et al., 1991a; Berson et al., 2002). Future studies will have to evaluate the effect of the *F45L* mutation on rhodopsin dimerization *in vivo* or use alternative or complementary methods of disrupting rhodopsin dimers (Jastrzebska et al., 2006; Getter et al., 2021) to further investigate the possible role of allosteric interactions between rhodopsin monomers in disk membranes in photoreceptor signaling.

## References

- Arshavsky VY, Burns ME (2014) Current understanding of signal amplification in phototransduction. *Cell Logist* 4:e29390.
- Arshavsky VY, Lamb TD, Pugh EN Jr (2002) G proteins and phototransduction. *Annu Rev Physiol* 64:153–187.
- Baylor DA, Lamb TD, Yau KW (1979) Responses of retinal rods to single photons. *J Physiol* 288:613–634.
- Berson EL, Rosner B, Weigel-DiFranco C, Dryja TP, Sandberg MA (2002) Disease progression in patients with dominant retinitis pigmentosa and rhodopsin mutations. *Invest Ophthalmol Vis Sci* 43:3027–3036.
- Choe HW, Kim YJ, Park JH, Morizumi T, Pai EF, Krauss N, Hofmann KP, Scheerer P, Ernst OP (2011) Crystal structure of metarhodopsin II. *Nature* 471:651–655.
- Cordomi A, Perez JJ (2009) Structural rearrangements of rhodopsin subunits in a dimer complex: a molecular dynamics simulation study. *J Biomol Struct Dyn* 27:127–147.
- Ernst OP, Gramse V, Kolbe M, Hofmann KP, Heck M (2007) Monomeric G protein-coupled receptor rhodopsin in solution activates its G protein transducin at the diffusion limit. *Proc Natl Acad Sci USA* 104:10859–10864.
- Fotiadis D, Jastrzebska B, Philippsen A, Muller DJ, Palczewski K, Engel A (2006) Structure of the rhodopsin dimer: a working model for G-protein-coupled receptors. *Curr Opin Struct Biol* 16:252–259.
- Frederiksen R, Nymark S, Kolesnikov AV, Berry JD, Adler L, Koutalos Y, Kefalov VJ, Cornwall MC (2016) Rhodopsin kinase and arrestin binding control the decay of photoactivated rhodopsin and dark adaptation of mouse rods. *J Gen Physiol* 148:1–11.
- Fulton AB, Hansen RM, Moskowitz A (2009) Development of rod function in term born and former preterm subjects. *Optom Vis Sci* 86:E653–E658.

- Getter T, Kemp Vinberg F, Palczewski K (2021) Identification of small-molecule allosteric modulators that act as enhancers/disrupters of rhodopsin oligomerization. *J Biol Chem* 297:101401.
- Jastrzebska B, Fotiadis D, Jang GF, Stenkamp RE, Engel A, Palczewski K (2006) Functional and structural characterization of rhodopsin oligomers. *J Biol Chem* 281:11917–11922.
- Kaushal S, Khorana HG (1994) Structure and function in rhodopsin. 7. Point mutations associated with autosomal dominant retinitis pigmentosa. *Biochemistry* 33:6121–6128.
- Kolesnikov AV, Rikimaru L, Hennig AK, Lukasiewicz PD, Fliesler SJ, Govardovskii VI, Kefalov VJ, Kisselev OG (2011) G-protein beta-gamma-complex is crucial for efficient signal amplification in vision. *J Neurosci* 31:8067–8077.
- Kolesnikov AV, Orban T, Jin H, Brooks C, Hofmann L, Dong Z, Sokolov M, Palczewski K, Kefalov VJ (2017) Dephosphorylation by protein phosphatase 2A regulates visual pigment regeneration and the dark adaptation of mammalian photoreceptors. *Proc Natl Acad Sci U S A* 114:E9675–E9684.
- Kota P, Reeves PJ, Rajbhandary UL, Khorana HG (2006) Opsin is present as dimers in COS1 cells: identification of amino acids at the dimeric interface. *Proc Natl Acad Sci U S A* 103:3054–3059.
- Lamb TD, Pugh EN Jr (2004) Dark adaptation and the retinoid cycle of vision. *Prog Retin Eye Res* 23:307–380.
- Lem J, Krasnoperova NV, Calvert PD, Kosaras B, Cameron DA, Nicolo M, Makino CL, Sidman RL (1999) Morphological, physiological, and biochemical changes in rhodopsin knockout mice. *Proc Natl Acad Sci U S A* 96:736–741.
- Lewis TR, Shores CR, Cady MA, Hao Y, Arshavsky VY, Burns ME (2020) The F220C and F45L rhodopsin mutations identified in retinitis pigmentosa patients do not cause pathology in mice. *Sci Rep* 10:7538.
- Palczewska G, Stremplewski P, Suh S, Alexander N, Salom D, Dong Z, Ruminski D, Choi EH, Sears AE, Kern TS, Wojtkowski M, Palczewski K (2018) Two-photon imaging of the mammalian retina with ultrafast pulsing laser. *JCI Insight* 3:e121555.
- Palczewski K (2006) G protein-coupled receptor rhodopsin. *Annu Rev Biochem* 75:743–767.
- Park JH, Scheerer P, Hofmann KP, Choe HW, Ernst OP (2008) Crystal structure of the ligand-free G-protein-coupled receptor opsin. *Nature* 454:183–187.
- Ploier B, Caro LN, Morizumi T, Pandey K, Pearring JN, Goren MA, Finnemann SC, Graumann J, Arshavsky VY, Dittman JS, Ernst OP, Menon AK (2016) Dimerization deficiency of enigmatic retinitis pigmentosa-linked rhodopsin mutants. *Nat Commun* 7:12832.
- Pugh EN Jr, Lamb TD (1993) Amplification and kinetics of the activation steps in phototransduction. *Biochim Biophys Acta* 1141:111–149.
- Rieke F (2000) Mechanisms of single-photon detection in rod photoreceptors. *Methods Enzymol* 316:186–202.
- Rivero-Muller A, Chou YY, Ji I, Lajic S, Hanyaloglu AC, Jonas K, Rahman N, Ji TH, Huhtaniemi I (2010) Rescue of defective G protein-coupled receptor function in vivo by intermolecular cooperation. *Proc Natl Acad Sci U S A* 107:2319–2324.
- Salom D, Lodowski DT, Stenkamp RE, Le Trong I, Golczak M, Jastrzebska B, Harris T, Ballesteros JA, Palczewski K (2006) Crystal structure of a photoactivated deprotonated intermediate of rhodopsin. *Proc Natl Acad Sci U S A* 103:16123–16128.
- Scheerer P, Park JH, Hildebrand PW, Kim YJ, Krauss N, Choe HW, Hofmann KP, Ernst OP (2008) Crystal structure of opsin in its G-protein-interacting conformation. *Nature* 455:497–502.
- Sokolov M, Lyubarsky AL, Strissel KJ, Savchenko AB, Govardovskii VI, Pugh EN Jr, Arshavsky VY (2002) Massive light-driven translocation of transducin between the two major compartments of rod cells: a novel mechanism of light adaptation. *Neuron* 34:95–106.
- Springael JY, Urizar E, Parmentier M (2005) Dimerization of chemokine receptors and its functional consequences. *Cytokine Growth Factor Rev* 16:611–623.
- Sung CH, Davenport CM, Hennessey JC, Maumenee IH, Jacobson SG, Heckenlively JR, Nowakowski R, Fishman G, Gouras P, Nathans J (1991a) Rhodopsin mutations in autosomal dominant retinitis pigmentosa. *Proc Natl Acad Sci U S A* 88:6481–6485.
- Sung CH, Schneider BG, Agarwal N, Papermaster DS, Nathans J (1991b) Functional heterogeneity of mutant rhodopsins responsible for autosomal dominant retinitis pigmentosa. *Proc Natl Acad Sci U S A* 88:8840–8844.
- Tsukamoto H, Sinha A, DeWitt M, Farrens DL (2010) Monomeric rhodopsin is the minimal functional unit required for arrestin binding. *J Mol Biol* 399:501–511.
- Urizar E, Montanelli L, Loy T, Bonomi M, Swillens S, Gales C, Bouvier M, Smits G, Vassart G, Costagliola S (2005) Glycoprotein hormone receptors: link between receptor homodimerization and negative cooperativity. *EMBO J* 24:1954–1964.
- Vinberg F, Kefalov V (2015) Simultaneous ex vivo functional testing of two retinas by in vivo electroretinogram system. *J Vis Exp* (99): e52855.
- Vincent AL, Carroll J, Fishman GA, Sauer A, Sharp D, Summerfelt P, Williams V, Dubis AM, Kohl S, Wong F (2013) Rhodopsin F45L allele does not cause autosomal dominant retinitis pigmentosa in a large Caucasian family. *Transl Vis Sci Technol* 2:4.
- Wang JS, Nymark S, Frederiksen R, Estevez ME, Shen SQ, Corbo JC, Cornwall MC, Kefalov VJ (2014) Chromophore supply rate-limits mammalian photoreceptor dark adaptation. *J Neurosci* 34:11212–11221.
- Wen XH, Shen L, Brush RS, Michaud N, Al-Ubaidi MR, Gurevich VV, Hamm HE, Lem J, Dibenedetto E, Anderson RE, Makino CL (2009) Overexpression of rhodopsin alters the structure and photoresponse of rod photoreceptors. *Biophys J* 96:939–950.
- Whorton MR, Bokoch MP, Rasmussen SG, Huang B, Zare RN, Kobilka B, Sunahara RK (2007) A monomeric G protein-coupled receptor isolated in a high-density lipoprotein particle efficiently activates its G protein. *Proc Natl Acad Sci U S A* 104:7682–7687.
- Whorton MR, Jastrzebska B, Park PS, Fotiadis D, Engel A, Palczewski K, Sunahara RK (2008) Efficient coupling of transducin to monomeric rhodopsin in a phospholipid bilayer. *J Biol Chem* 283:4387–4394.
- Woodruff ML, Lem J, Fain GL (2004) Early receptor current of wild-type and transducin knockout mice: photosensitivity and light-induced Ca<sup>2+</sup> release. *J Physiol* 557:821–828.
- Yue WWS, Silverman D, Ren X, Frederiksen R, Sakai K, Yamashita T, Shichida Y, Cornwall MC, Chen J, Yau KW (2019) Elementary response triggered by transducin in retinal rods. *Proc Natl Acad Sci U S A* 116:5144–5153.
- Zhao DY, Poge M, Morizumi T, Gulati S, Van Eps N, Zhang J, Miszta P, Filipek S, Mahamid J, Plitzko JM, Baumeister W, Ernst OP, Palczewski K (2019) Cryo-EM structure of the native rhodopsin dimer in nanodiscs. *J Biol Chem* 294:14215–14230.